SCIENCE CHINA
Information Sciences

• RESEARCH PAPER •

July 2026, Vol. 69, Iss. 7, 170403:1–170403:8
https://doi.org/10.1007/s11432-025-4889-4

Special Topic: Advanced Optoelectronics Based on Two-Dimensional Materials

Strong optical emission regulated by exciton state in two-dimensional organic molecular crystals

Yutian YANG[1†], Ting ZHENG[2†], Weiwei ZHAO[1*], Chenyun CAO[1], Fang YANG[1*], Hongwei LIU[1*], Zhenhua NI[2,3] & Junpeng LU[2,3]

[1]*Key Laboratory of State Manipulation and Advanced Materials in Provincial Universities, School of Physics and Technology, Nanjing Normal University, Nanjing 210046, China*
[2]*Key Laboratory of Quantum Materials and Devices of Ministry of Education, School of Physics, Southeast University, Nanjing 211189, China*
[3]*School of Electronic Science and Engineering, Southeast University, Nanjing 210096, China*

Received 25 December 2025/Revised 11 February 2026/Accepted 30 March 2026/Published online 23 June 2026

Abstract The strong transition dipole-dipole interaction in two-dimensional organic molecular crystals induces the exciton effect between electron and hole spins, resulting in the splitting of the bright exciton state and the dark exciton state. The modulation of bright and dark exciton states has aroused great interest in the field of quantum information applications. Conventional thermally activated delayed fluorescence materials, which rely on spatially separated donor-acceptor structures, often exhibit broad emission spectra and efficiency roll-off. In this work, we demonstrate a temperature-induced transition from dark to bright exciton states within the wetting layer of a two-dimensional organic crystal. By switching the aggregation mode from H-aggregation to Hj-aggregation at low temperature, the non-radiative triplet-like states are effectively converted into radiative singlet-like states. This leads to a remarkable enhancement of the photoluminescence quantum yield and the emergence of superradiance, manifested as an intensified 0-0 emission band and a narrowed linewidth. We thus establishes a strategy for achieving flexible switching between bright and dark exciton states through precise control of molecular packing, which enables the design of specific Hj-aggregates with tailored excited-state coherence. This superradiant system, featuring large oscillator strengths and tunable excitonic properties, provides a new platform for quantum information processing.

Keywords two-dimensional materials, organic crystal, aggregation, exciton state, superradiance

Citation Yang Y T, Zheng T, Zhao W W, et al. Strong optical emission regulated by exciton state in two-dimensional organic molecular crystals. Sci China Inf Sci, 2026, 69(7): 170403, https://doi.org/10.1007/s11432-025-4889-4

1 Introduction

Two-dimensional organic crystals (2D OCs) are characterized by their layer-by-layer assembly from conjugated molecules via van der Waals interactions, which endow them with ultrathinness, flexibility, and processability, which are key to their promise in advanced displays and optoelectronics [1–5]. 2D OCs have stronger dipole-dipole interactions; also, quantum and dielectric confinement in the ultimate 2D limit greatly enhance excitonic effects [6–9]. The exchange interaction between the electron and hole spins induces a splitting of excitonic states into the bright and dark exciton states, driven by molecular transition dipole-dipole interactions [10–12]. In dark exciton states, electrons and holes possess parallel spins, violating spin momentum conservation and preventing direct photon emission upon recombination [13, 14]. Consequently, dark excitons exhibit considerably longer radiative lifetimes compared to bright excitons. Their high stability and non-radiative nature make them attractive for applications such as quantum information processing, Bose-Einstein condensation, and light-harvesting systems [15, 16]. Compared with dark excitons, electrons and holes in the bright exciton state have anti-parallel spins, allowing efficient recombination via photon emission. The spontaneous coherent emission of bright excitons can cause superradiance and has significant applications in on-chip optical communication, transient light-emitting devices, and high-quantum yield organic light-emitting diode (OLED) [17–19].

The modulation of bright and dark exciton states has aroused great interest in the field of quantum information applications [20, 21]. Adachi et al. innovatively designed a thermally activated delayed fluorescence (TADF)

* Corresponding author (email: jianpiao1986@163.com, phyyf@nnu.edu.cn, phylhw@njnu.edu.cn)
† These authors contributed equally to this work.

material with an extremely small singlet-triplet energy gap, enhancing the crossover between triplet-singlet reverse systems [22]. Due to the fact that TADF materials rely on the spatially separated the donor-acceptor (D-A) structure, the excited-state charge transfer (CT) characteristics are obvious, resulting in problems such as spectral broadening, efficiency roll-off, and poor color purity [23]. Therefore, new OLED luminescent materials that achieve narrow-spectrum emission and high exciton utilization have become the focus of research [24]. The weakened screening effect in 2D OCs leads to a significant enhancement of dipole-dipole interactions, making the behavior of the Frenkel exciton highly dependent on intermolecular interactions induced by molecular aggregation [25]. Dicke was the first to predict the superradiance phenomenon induced by the spontaneous coherent radiance atoms in aggregates, and it was successively confirmed in J-aggregates [26–28]. But in H-aggregates, where dark excitons reside at the bottom of the exciton band, radiative decay to the ground state via direct luminescence is typically forbidden [13]. Therefore, inducing a dark exciton state to a bright exciton state is a novel direction for enhancing the quantum efficiency of materials [29]. However, the transition of the molecular aggregation to regulate exciton behavior is regarded as challenging, as it usually requires altering the molecular crystal structure. Consequently, precise control over the packing motifs of molecular crystals offers a promising route to modulate excitonic coupling and generate novel optoelectronic properties [30–32].

Here, using 2,7-Dioctyl[1]benzothieno[3,2-b][1]benzothiophene (C8-BTBT) molecular crystals as a model system, we systematically investigate the unique excitonic behaviors in 2D molecular aggregates. Benefiting from the distinct Coulomb coupling environment within the wetting layer (WL) crystalline, we observe a series of distinctive transitions from dark to bright exciton states. Through the temperature dependent photoluminescence spectroscopy, time-resolved fluorescence spectroscopy, and polarization-resolved spectroscopy, we have studied the influence of temperature on exciton coherence length, radiative recombination rate, and the superradiance effect.

2 Characterization and room-temperature optical properties

Utilizing the gradient control of substrate temperature in physical vapor deposition (PVD), we synthesize a series of 2D C_8-BTBT organic crystalline films with various thicknesses (Figure 1(a) and Supplementary Note 1). The transition dipole moment (TDM) of a single C_8-BTBT molecule and the structure diagram of WL and 1L on hexagonal boron nitride (h-BN) substrates are shown in Figure 1(b). In the Kasha model, the type of molecular aggregation is primarily determined by the nearest-neighbor molecules' Coulomb coupling (J_{Coul}), which is determined by the alignment of their TDM [25],

$$J_{\mathrm{Coul}} \approx \frac{\mu^2(\cos\alpha - 3\cos\theta_1\cos\theta_2)}{4\pi\varepsilon R^3}, \tag{1}$$

where R is the intermolecular distance between mass centers, μ is the transition dipole moment, θ_1 and θ_2 are the angle between μ and R, and ε is the optical dielectric constant of the medium. According to our previous research, the nearest-neighbor coupling in WL C_8-BTBT organic crystals is positive ($J_{\mathrm{Coul}} > 0$) and the next-nearest-neighbor coupling is negative ($J_{\mathrm{Coul}} < 0$) [33]. The nearest-neighbor coupling in 1L C_8-BTBT organic crystals is negative ($J_{\mathrm{Coul}} < 0$), which enables the formation of J-agggregates through intra-chain Coulombic interactions. Optical micrographs and atomic force microscopy (AFM) images of WL on the h-BN substrate (before and after growth) are shown in Figures 1(c) and (d). The height of WL is approximately 0.6 nm in Figure 1(d), consistent with previous reports [33]. The height profiles for the 1L, 2L, and 3L samples (Figures 1(e) and S1) show step heights of ∼3 nm, corresponding to the expected thickness for layers with an in-plane herringbone packing.

Different from the molecular structure found in previous studies [34–36], the molecular arrangement starting from 1L becomes more upright. This is mainly due to the significant reduction in the adsorption energy between the substrates after the oxygen plasma pre-treatment of the substrates (Figure S2 and Supporting information Note 1). Compared with the optical microscope images, the contrast spectra image can clearly observe the morphologies of WL and 1L before and after growth on h-BN, as shown in Figures 1(f) and (g). The optical contrast spectra of WL and 1L before (C_0) and after (C_1) growth on the h-BN substrate are shown in Figures 1(h) and (i), respectively. The differential optical contrast spectrum for the WL (orange circle) is calculated as $C' = C_0 - C_1 = \Delta R/R$, where ΔR is the differential reflectance and R is the substrate reflectance. The optical contrast spectrum of the C_8-BTBT molecular crystal is similar to a wavelength diffraction pattern throughout the visible light range, with a negative contrast value in the 420–530 nm range and a positive contrast value in the 530–740 nm range. Figure S3 displays the contrast spectra for the WL to 5L films, clearly showing that the characteristic peak amplitudes increase with layer number. Therefore, the layer count can be determined by comparing these characteristic peaks, offering a rapid and non-destructive method.

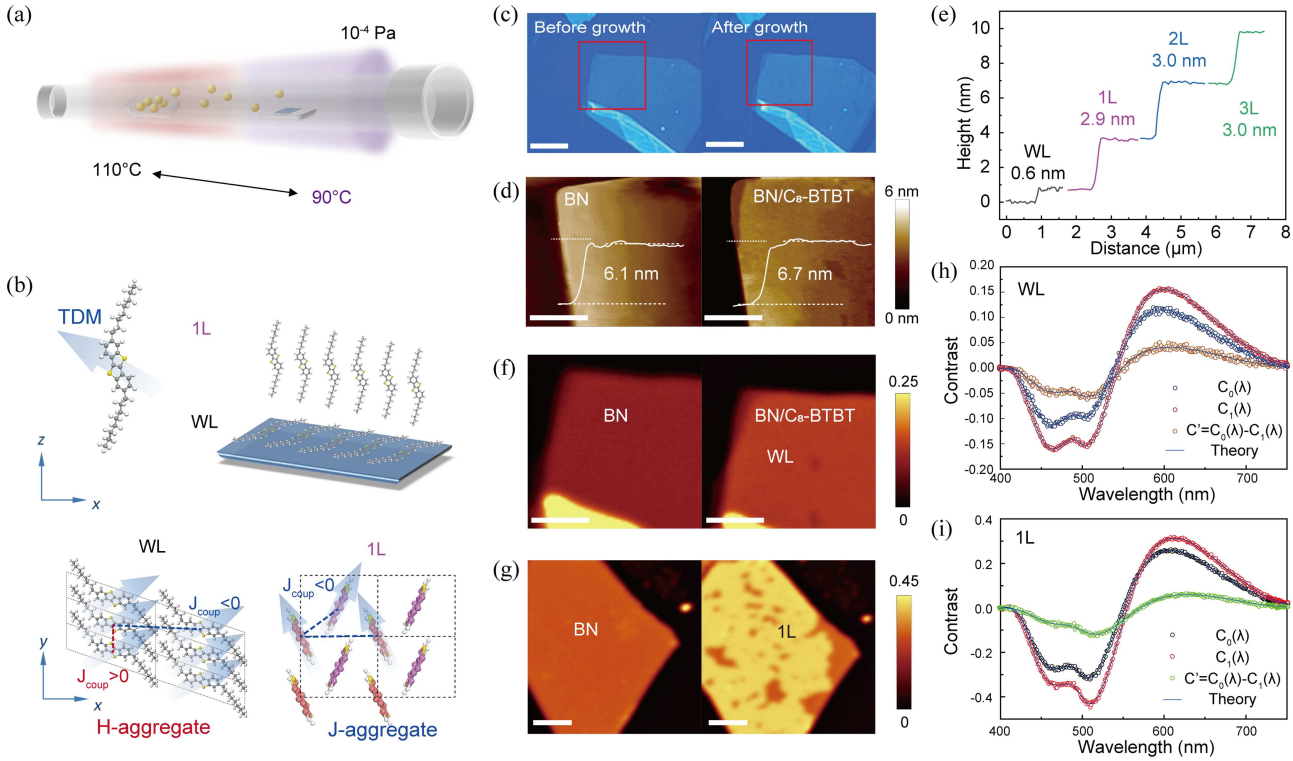

Figure 1 (Color online) (a) PVD process of 2D C_8-BTBT molecular crystals. (b) In-plane molecular packing of ML and 1L C_8-BTBT on h-BN. (c) Optical micrographs and (d) AFM images of WL before (left) and after (right) growth on h-BN. (e) Height profiles for the WL, 1L, 2L, and 3L C_8-BTBT molecular crystals. Contrast spectra image of (f) WL and (g) 1L. Scale bars: 10 μm. Optical contrast spectrum of (h) WL and (i) 1L measured from (f) and (g).

In most π-conjugated organic molecules, a strong vibrational coupling exists between the $S_0 \rightarrow S_1$ optical transition and the vinyl ring stretching mode (~1500 cm^{-1}) [37]. The C_8-BTBT crystal spectrum shows its characteristic peaks at 1147 and 1475 cm^{-1}, as shown in Figure S4. This coupling arises because the electronic excitation alters the π-bond order, which directly modulates the vibrational coordinates of the conjugated backbone. This coupling also results in a significant vibrational fine structure in the absorption and photoluminescence (PL) spectra of the isolated chromophore (monomer), as shown in Figure S5. When these chromophores interact electronically to form aggregates, the progression becomes distorted, and the relative peak intensities deviate from the Poisson distribution characteristic of monomers. Therefore, we further investigated the optical properties of the molecular aggregates using PL spectroscopy at room temperature. Figure 2(a) illustrates the PL spectra of C_8-BTBT in solution (monomer) and for the different layered films. Well-resolved peaks corresponding to the pure electronic (0-0) transition and vibronic progressions (0-1, 0-2, etc.) are observed. Compared to the monomer spectrum in solution, the PL spectra of the aggregates show a distinct redshift. This redshift is not solely due to the energy band splitting caused by long-range Coulomb coupling in monomers but arises from the coupling between Frenkel excitons and intermolecular CT excitons under resonant conditions in the aggregates. According to the Franck-Condon principle, the intensity ratio of the first two PL peaks ($I_{0\text{-}0}$ and $I_{0\text{-}1}$) directly reflects the strength of the electron-vibrational coupling. As shown in Figure 2(b), the integrated intensity ratio ($R_{01} = I_{0\text{-}0}/I_{0\text{-}1}$) for the H-aggregate WL is 0.75, indicating that the 0-0 transition is not completely forbidden, due to the weak coupling in WL H-aggregates at room temperature, where the 0-0 peak is thermally activated [38]. Significant 0-0 and 0-1 transitions were observed in J-aggregate crystals, where the 0-1 transition intensity (relative to the 0-0 transition intensity) steadily increased with increasing the number of crystal layers until it eventually approached or even exceeded the 0-0 peak. For the J-aggregate crystalline films (1L–5L, bulk), the R_{01} gradually decreases with increasing layer number. This can be attributed to the larger in-plane electronic coupling and interlayer CT states as the molecular layers increase, resulting in a reduction of 0-0 transitions [28]. Furthermore, polarization-resolved PL spectra reveal anisotropic emission with a 180° periodicity for the WL, 1L, and monomer C_8-BTBT (Figure 2(c)). At room temperature, the degree of polarization in 1L ($P = (I_{max} - I_{min})/(I_{max} + I_{min}) = 25\%$) is greater than that in WL ($P = 14\%$). This indicates that the influence of thermal disturbance on the molecular polarization of the H-aggregate is more obvious. It is worth noting that there are no obvious polarization characteristics in monomer molecules, which also

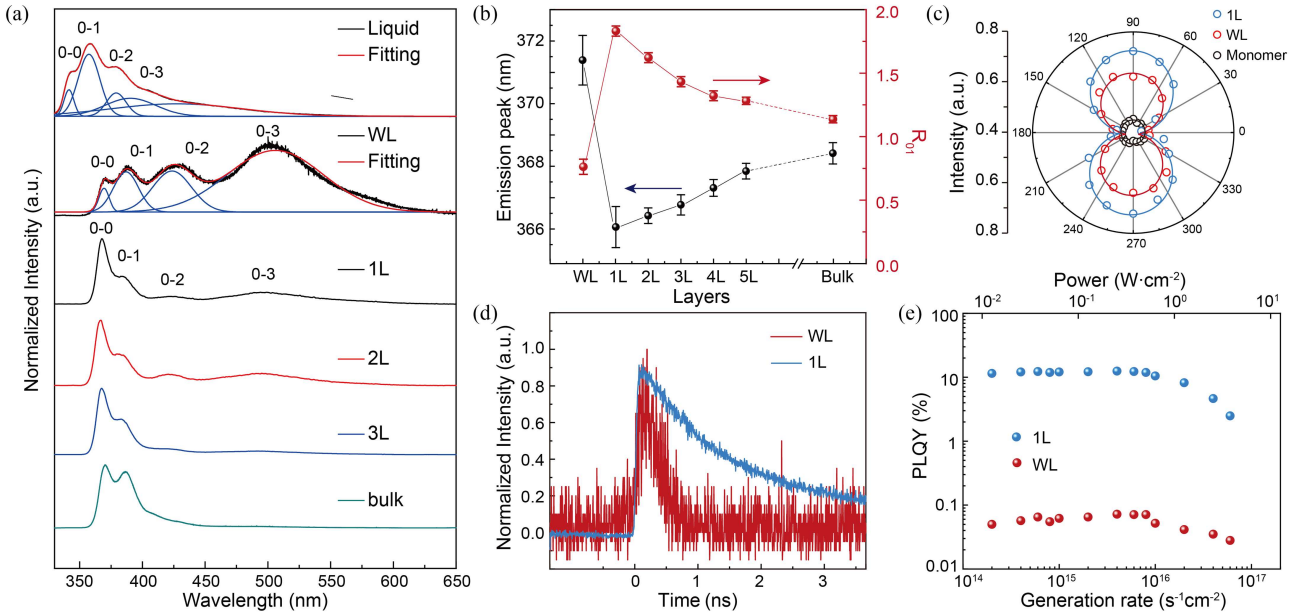

Figure 2 (Color online) (a) The PL spectra for monomer, WL, 1L, 2L, 3L, and bulk C_8-BTBT molecular samples. (b) The peak position and R_{01} of a series of layers of C_8-BTBT crystals. (c) Angle-resolved PL for WL (red), 1L (black), and monomer (blue) C_8-BTBT samples. (d) Time-resolved PL between WL and 1L. The lifetimes of 720 ps and 2.4 ns at WL and 1L were extracted, respectively, by using biexponential fitting. (e) PLQY of WL and 1L C_8-BTBT crystals as a function of pump power (optical generation rate).

indicates that polarization mainly originates from molecular aggregates.

We perform time-resolved photoluminescence (TRPL) measurements to study the exciton lifetimes in the WL and 1L C_8-BTBT crystals. Figure 2(d) shows the PL lifetime of the WL and 1L C_8-BTBT crystal, and it can be fitted with both faster and slower components. The faster component is attributed to radiative recombination, and the slower component can be non-radiative due to traps or disorder, which contribute less to the total excitation. The lifetime of the faster component in the WL C_8-BTBT crystal is 720 ps, significantly shorter than the 2.4 ns lifetime observed for the 1L. This illustrates that the PL lifetime in the WL C_8-BTBT crystal is dominated by the CT state with a shorter lifetime. On the other hand, the CT state of exciton delocalization caused by the thermal effect also eliminates the 0-0 transition barrier in H-aggregates, allowing the relatively weak 0-0 transition PL in the WL C_8-BTBT crystal to be observed at room temperature. We also measured the room temperature photoluminescence quantum yield (PLQY) of the WL and 1L C_8-BTBT crystal under 355 nm excitationm as shown in Figure 2(e). Under low injection, the PLQY of 1L is approximately 10%, while, in contrast, this value in WL is only below 0.1%. This is due to the dominant intralayer CT and H-aggregation effects in the WL C_8-BTBT crystal. The dark excitons reside at the bottom of the exciton band in H-aggregates; radiative decay to the ground state is typically forbidden. Therefore, in an ideal H-aggregated molecular crystal, the corresponding 0-0 transition band has no fluorescence emission. However, due to the existence of CT states within the WL layer, the secondary CT transport mechanism results in relatively weak fluorescence production. Time-resolved PL also confirmed that short-lived CT exciton processes can be observed in the WL. At a high generation rate (up to 10^{10} s^{-1}·cm^{-2}), excitons cannot be rapidly released through radiative recombination. This causes a local temperature increase in the organic crystal, which may enhance the electron-phonon coupling and increase the non-radiative recombination channels, thereby significantly reducing the PLQY.

3 Temperature-dependent optical properties

To further investigate the exciton properties, we conduct temperature-dependent PL measurements. Figures 3(a) and (b) show the temperature-dependent PL spectra of the WL and 1L C_8-BTBT crystal, respectively. With the decrease in temperature, the emission intensity in the 0-0 band (∼375 nm) significantly increases, while the linewidth and vibration order decrease. This temperature-dependent narrowing of the exciton emission linewidth is primarily attributed to the reduction in dynamic disorder. As the temperature decreases, electron-phonon coupling is suppressed, and thermal lattice vibrations weaken, thereby significantly reducing the dynamic disorder induced by phonon scattering. This enhances the phase coherence of excitons and increases their coherence length. Thus,

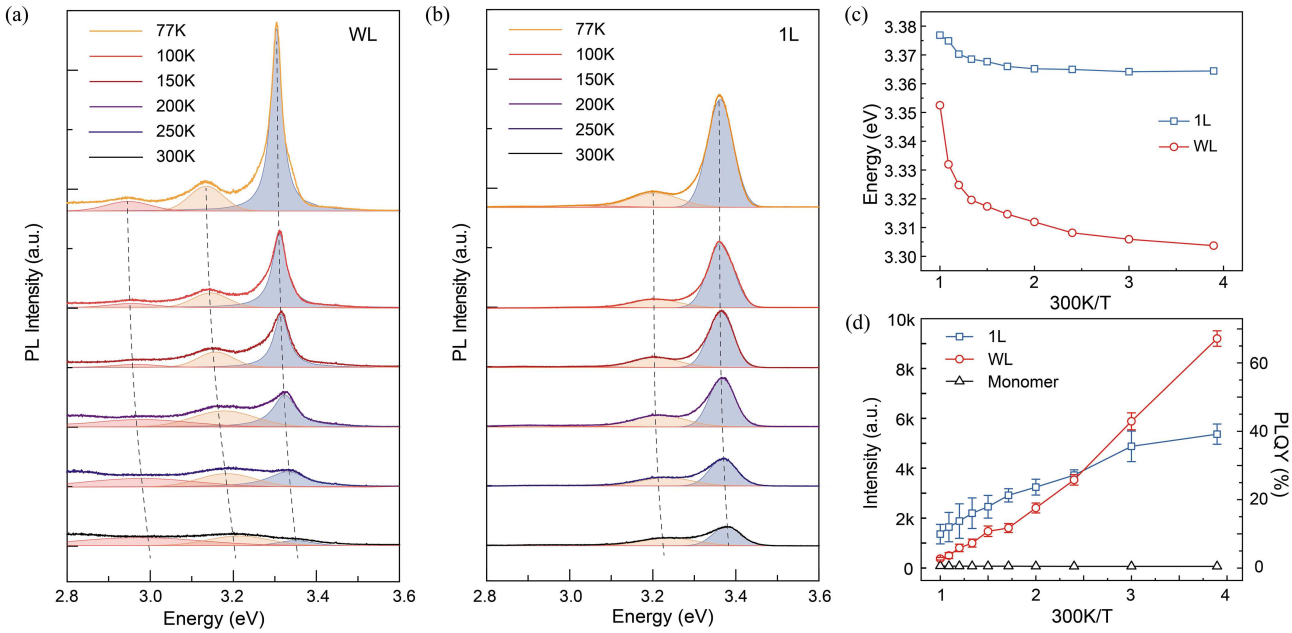

Figure 3 (Color online) Temperature-dependent PL spectra of the WL (a) and 1L (b) C_8-BTBT crystals. (c) The variation of the 0-0 band emission peak positions of the WL and 1L C_8-BTBT crystals with temperature. (d) The temperature dependence of the 0-0 band emission intensity and PLQY for the WL, 1L, and monomer samples.

the linewidth narrowing serves as a direct optical signature of reduced dynamic disorder, which is consistent with the observed redshift of the 0-0 band and the increase in the R_{01} intensity ratio, indicating an increased coherence length in aggregated crystals at lower temperatures (Figures S6 and S7). The behavior in H-aggregates may be more complex, as temperature-induced disorder can also affect the intensity of the symmetry-forbidden transition, with the R_{01} increasing as the temperature increases. The redshift of the PL emission band can be observed in WL and 1L C_8-BTBT crystal, as shown in Figures 3(c) and S8. There is a significantly stronger redshift in WL compared to 1L, reflecting that, apart from thermal disturbances, there may be other processes that cause changes in the band structure.

The temperature-dependent PL intensity and PLQY of WL, 1L are plotted in Figures 3(d) and S9. Under thermodynamic equilibrium, the PL intensity of the 0-0 emission is proportional to the square of the thermal coherent number N_T. We find that the WL reaches $N_T = 78$ (9×9), while for the 1L film $N_T = 37$ (6×6) gives reasonably good agreement with experimental data. At room temperature (300 K), the coherent number decreases markedly due to thermal disordering $N_T = 3$ (2×2) for the WL and $N_T = 9$ (3×3) for the 1L film. In contrast, monomer C_8-BTBT on amorphous SiO_2 substrates showed no significant increase in the 0-0 emission intensity at low temperature. The PLQY for the WL can reach up to 62% at 77 K, which is more than two orders of magnitude higher than that at room temperature. The WL C_8-BTBT crystal has lower defect density, allowing excitons to delocalize over hundreds of molecules, thereby enabling the observation of a size-dependent superradiance effect based on macroscopic coherence at cryogenic temperatures.

4 Theoretical modeling

We rationalized our experimental results theoretically using a Hamiltonian of pristine aggregates derived from first-principles calculations. As illustrated in Figure 4(a), with the decrease in temperature, the aggregation state of molecules in WL transitions from H-aggregation to Hj-aggregation. This is because the Frenkel excitons in WL are tightly bound around the molecule at room temperature, and only the adjacent transition dipoles form coherent interactions. On the other hand, at low temperatures, the increase in coherence length leads to an enhancement of the transition dipole coherence effect of the next nearest neighbors. The molecules in WL aggregate to form the Hj-aggregation state at low temperatures, which is completely different from the H-aggregation state at room temperature. As a result, the dark excitons in the 0-0 exciton band of WL transform into bright excitons (Figures 4(b) and S6), which is a rare occurrence in aggregated molecular systems.

To better understand the influence of temperature on the thermal coherence number and the change of exciton

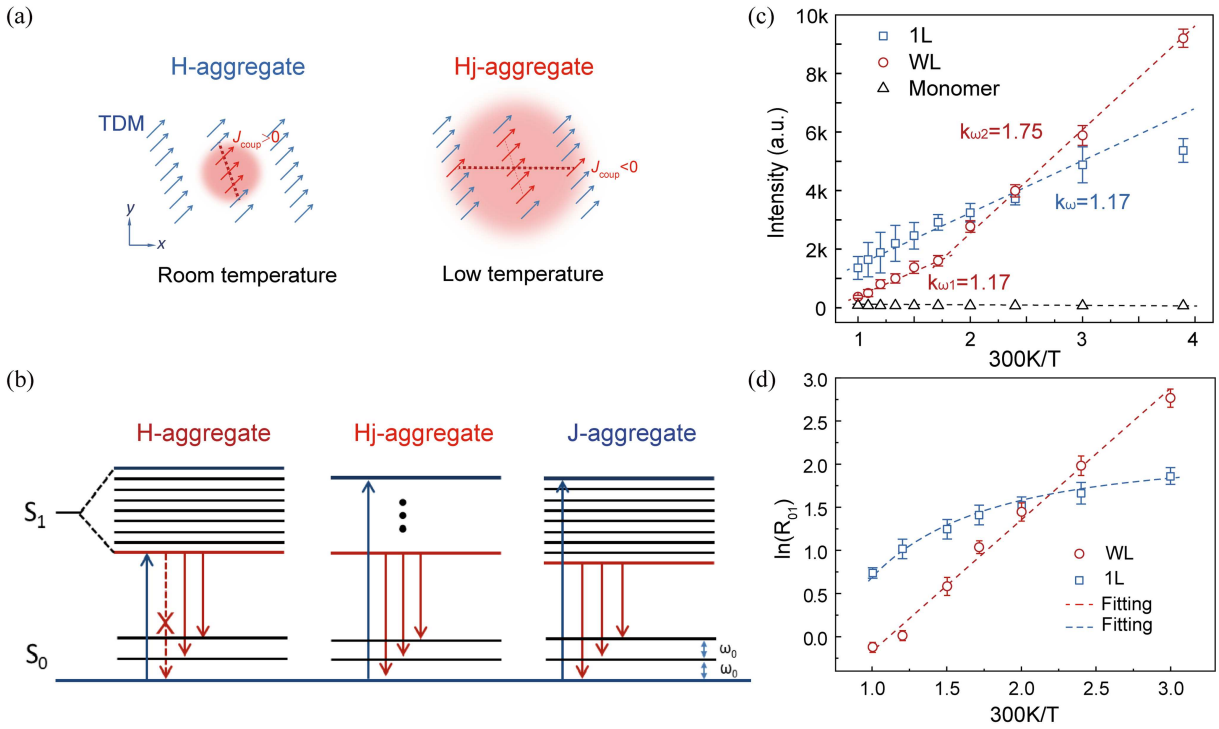

Figure 4 (Color online) (a) The spatial distribution of the lowest excited state in a small cluster (lower left) and large aggregate (right) in WL. The red and blue arrows denote the transition dipole moments of excited and unexcited single molecules. (b) Schematic illustration of the excitonic band diagram of WL and 1L C_8-BTBT crystals. (c) The temperature dependence of the PL emission intensity as a function of inverse temperature for WL, 1L, and monomer samples. (d) The ratio $\ln(R_{01})$ as a function of inverse temperature for WL and 1L C_8-BTBT crystals.

state, the relationship between N_T and temperature can be given as follows [39]:

$$N_T \cong 1 + \frac{4\pi\hbar\omega_C}{kT}, \tag{2}$$

where k is the Boltzmann constant and ω_C is the band curvature defined in the continuum limit. The expression of ω_C can also be given as follows:

$$\omega_C = \frac{\hbar}{2d^2 m_{\text{eff}}}, \tag{3}$$

where d is the wave vector index and the m_{eff} is the effective mass of the exciton. According to (2), the temperature-dependent PL intensity and ω_C at the 0-0 band are plotted in Figure 3(c). Comparing the experimental PL intensity of the 1L films with the theoretical fit based purely on thermal effects reveals excellent agreement. The thermal interaction leads to an increase in the effective mass of excitons (the slope of ω_C is $k_\omega = 1.17$), which limits the delocalization of excitons and reduces the number of coherent emission molecules. For WL, two linear curves can be used for fitting, corresponding respectively to H-aggregation ($k_\omega = 1.17$) and Hj-aggregation ($k_\omega = 1.75$). The critical transition temperature is 175 K ($N = 6$, lattice size is 2×3), at which point the excited molecule happens to interact coherently with the transition dipole of the next neighboring molecule. At ultra-low temperatures, WL C_8-BTBT crystals can form more coherent dipole interactions (suggesting that N_T can reach the order of 200 at zero temperature), which is called supercoherence.

Importantly, the 0-0 band and the 0-1 band show different temperature dependence; in fact, the 0-0 band intensity has a stronger temperature dependence. This is clearly shown in Figure 4(d), where the temperature dependence of the $\ln(R_{01})$ of WL and 1L C_8-BTBT crystals is shown. In WL, the $\ln(R_{01})$ varies significantly with $1/T$ and can be linearly fitted, which is a typical feature of superradiance. The coherent interactions of many Frenkel dipoles form a huge superradiant transition dipole, which mainly emits in the 0-0 band. However, the trend in 1L gradually slows down, which reflects that the superradiant effect in J-aggregation is no longer dominant. It is the result of the competition between the CT state and the coherent dipole interaction in the J-aggregation. At higher temperatures (typically >100 K for aggregates), coherent radiation is primarily limited by phonon scattering. At very low temperatures (<100 K), it is limited mainly by static disorder induced by structural defects and impurities. This also explains the deviation of the PL of 1L from the theoretical prediction at low temperatures in Figure 4(c).

5 Conclusion

In summary, we report a series of unique transitions of WL C_8-BTBT crystals from dark exciton states to bright exciton states at low temperatures. The strong coherence of transitioning dipole molecules at low temperatures leads to the change of bright and dark exciton states, which can be attributed to the transformation from H-aggregation to Hj-aggregation in WL. It shows the PLQY as high as 62% at 77 K, and the temperature dependence of PL intensity, exciton line width, and $R_{0\text{-}1}$ provide evidence of superradiance. It is demonstrated that the coherence and radiation efficiency of excitons can be effectively manipulated through organic aggregation engineering and temperature control, providing a theoretical platform for the development of low-temperature photodetectors, high-efficiency OLEDs, and quantum information devices.

Acknowledgements This work was supported by National Key Research and Development Program of China (Grant No. 2024YFE0217500) and National Natural Science Foundation of China (Grant Nos. U25A20511, 12274234, 62404105).

Supporting information Appendix A. The supporting information is available online at info.scichina.com and link.springer.com. The supporting materials are published as submitted, without typesetting or editing. The responsibility for scientific accuracy and content remains entirely with the authors.

References

1 Liu K, Jiang Y, Liu F, et al. Organic solar cells with over 19% efficiency enabled by a 2d-conjugated non-fullerene acceptor featuring favorable electronic and aggregation structures. Adv Mater, 2023, 35: e2300363
2 Li W, Ren X, He M, et al. High-brightness blue-emission crystalline thin-film OLEDs based on thick solid-solution emitting layer. Laser Photonics Rev, 2025, 20: e02043
3 Shi Y, Jiang L, Liu J, et al. Bottom-up growth of n-type monolayer molecular crystals on polymeric substrate for optoelectronic device applications. Nat Commun, 2018, 9: 2933
4 Wang C, Dong H, Jiang L, et al. Organic semiconductor crystals. Chem Soc Rev, 2018, 47: 422–500
5 Wang Q, Juarez-Perez E J, Jiang S, et al. Spin-coated crystalline molecular monolayers for performance enhancement in organic field-effect transistors. J Phys Chem Lett, 2018, 9: 1318–1323
6 Dou D, Shi Q, Li H, et al. Rational combination of π-conjugated and non-π-conjugated groups achieving strong nonlinear optical response, large optical anisotropy, and UV light-switchable fluorescence. Adv Sci, 2024, 11: e2401325
7 Sun J, Choi Y, Choi Y J, et al. 2D-organic hybrid heterostructures for optoelectronic applications. Adv Mater, 2019, 31: e1803831
8 Yang F, Cheng S, Zhang X, et al. 2D organic materials for optoelectronic applications. Adv Mater, 2018, 30: 1702415
9 An X, Zhang Y, Yu Y, et al. Efficient charge transfer in $WS_2/W_xMo_{1-x}S_2$ heterostructure empowered by energy level hybridization. Sci China Inf Sci, 2022, 66: 122404
10 Spano F C, Silva C. H- and J-aggregate behavior in polymeric semiconductors. Annu Rev Phys Chem, 2014, 65: 477–500
11 Sun H, Zhao Z, Spano F C, et al. Absorption and emission in quaterthienyl thin films. Adv Mater, 2003, 15: 818–822
12 Li W, Pan Y, Xiao R, et al. Employing ∼100% excitons in OLEDs by utilizing a fluorescent molecule with hybridized local and charge-transfer excited state. Adv Funct Mater, 2013, 24: 1609–1614
13 Hestand N J, Spano F C. Expanded theory of H- and J-molecular aggregates: the effects of vibronic coupling and intermolecular charge transfer. Chem Rev, 2018, 118: 7069–7163
14 Gierschner J, Lüer L, Milián-Medina B, et al. Highly emissive H-aggregates or aggregation-induced emission quenching? The photophysics of all-trans para-distyrylbenzene. J Phys Chem Lett, 2013, 4: 2686–2697
15 Zhang X X, You Y, Zhao S Y F, et al. Experimental evidence for dark excitons in monolayer WSe_2. Phys Rev Lett, 2015, 115: 257403
16 Kurdyubov A S, Trifonov A V, Gerlovin I Y, et al. Optical control of a dark exciton reservoir. Phys Rev B, 2021, 104: 035414
17 Liu C, Minari T, Lu X, et al. Solution-processable organic single crystals with bandlike transport in field-effect transistors. Adv Mater, 2011, 23: 523–526
18 Li L, Yu Y, Ye G J, et al. Black phosphorus field-effect transistors. Nat Nanotech, 2014, 9: 372–377
19 Qiu H, Yu Z H, Zhao T G, et al. Two-dimensional materials for future information technology: status and prospects. Sci China Inf Sci, 2024, 67: 160400
20 Hasan M M, Hume P A, Zhang L, et al. Excitonic dark states in molecular monolayer crystals. Nano Lett, 2025, 25: 383–390
21 Sun Q, Ren J, Jiang T, et al. Intermolecular charge-transfer-induced strong optical emission from herringbone H-aggregates. Nano Lett, 2021, 21: 5394–5400
22 Uoyama H, Goushi K, Shizu K, et al. Highly efficient organic light-emitting diodes from delayed fluorescence. Nature, 2012, 492: 234–238
23 Walia R, Xiong X, Fan X C, et al. Achieving small singlet-triplet energy gaps in polycyclic heteroaromatic emitters. Nat Mater, 2025, 24: 1576–1583
24 Zhang R, Gao J, Li N, et al. Circularly polarized organic light-emitting diode based on device functional layer materials. Small, 2025, 21: 2409541
25 Hestand N J, Spano F C. Molecular aggregate photophysics beyond the Kasha model: novel design principles for organic materials. Acc Chem Res, 2017, 50: 341–350
26 Spano F C, Mukamel S. Superradiance in molecular aggregates. J Chem Phys, 1989, 91: 683–700

27 Sun B, Xu X, Zhou G, et al. Observation of Strong J-aggregate light emission in monolayer molecular crystal on hexagonal boron nitride. J Phys Chem A, 2020, 124: 7340–7345

28 Zhao L, Wei Y, Zhang R, et al. Controlled surface oxidation of $HfSe_2$ via oxygen-plasma treatment. Mater Lett, 2019, 243: 96–99

29 Hestand N J, Spano F C. Molecular aggregate photophysics beyond the Kasha model: novel design principles for organic materials. Acc Chem Res, 2017, 50: 341–350

30 Wu B, Zhao Y, Nan H, et al. Precise, self-limited epitaxy of ultrathin organic semiconductors and heterojunctions tailored by van der Waals interactions. Nano Lett, 2016, 16: 3754–3759

31 Wang L, Li Q. Photochromism into nanosystems: towards lighting up the future nanoworld. Chem Soc Rev, 2018, 47: 1044–1097

32 Spano F C. Modeling disorder in polymer aggregates: the optical spectroscopy of regioregular poly(3-hexylthiophene) thin films. J Chem Phys, 2005, 122: 234701

33 Yang Y, Wang Y, Qiao J, et al. Aggregation-dependent dielectric permittivity in 2d molecular crystals. Small Methods, 2022, 6: 2101198

34 He D, Pan Y, Nan H, et al. A van der Waals pn heterojunction with organic/inorganic semiconductors. Appl Phys Lett, 2015, 107: 183103

35 He D, Zhang Y, Wu Q, et al. Two-dimensional quasi-freestanding molecular crystals for high-performance organic field-effect transistors. Nat Commun, 2014, 5: 5162–5167

36 He D, Qiao J, Zhang L, et al. Ultrahigh mobility and efficient charge injection in monolayer organic thin-film transistors on boron nitride. Sci Adv, 2017, 3: e1701186

37 Ghosh R, Spano F C. Excitons and polarons in organic materials. Acc Chem Res, 2020, 53: 2201–2211

38 Oleson A, Zhu T, Dunn I S, et al. Perylene diimide-based Hj- and hJ-aggregates: the prospect of exciton band shape engineering in organic materials. J Phys Chem C, 2019, 123: 20567–20578

39 Spano F C. Temperature-dependent emission in disordered herringbone aggregates of conjugated oligomers. Phys Rev B, 2005, 71: 235208